Journal of Marine Research, 54, 793–826, 1996

Journal of
MARINE RESEARCH

Volume 54, Number 5

Unsteady similarity solutions and oscillating ocean gyres

by Neil R. Edwards[1]

ABSTRACT

The effect of time-dependent forcing on steady solutions representing basin-scale flows is investigated. Analytical and numerical solutions are considered separately and compared.

We first use symmetry methods to show how any steady solution of the ideal thermocline equations can be used to generate a family of unsteady solutions, via an arbitrary function of time $\alpha(t)$. The resulting time-dependent solutions correspond to distortion of the isopycnal surfaces by a velocity field which varies linearly in the three coordinate directions. Although the displacements are linear, the fluctuations can lead to a form of nonlinear streaming wherever the function α appears nonlinearly in expressions for mass and heat fluxes. For an example steady solution, changes in internal energy caused by the time-dependence are associated with changes in thermocline depth and fluxes of energy from the western boundary, although it is unclear to what extent this behavior is specific to the example chosen. We also describe another symmetry of the time-dependent thermocline equations which generates wave-like solutions from arbitrary steady solutions. All the time-dependent solutions are special cases of a symmetry which applies to a general advection equation. Potential vorticity advection provides another special case.

With the inclusion of convective and dissipative processes, a more realistic steady solution is found numerically in a flat-bottomed sector. If the surface forcing functions oscillate annually, the resulting flow resembles the analytical predictions. As the oscillation period increases, spatial variations in phase disrupt the agreement as first boundary and then diffusive effects become important. For decadal period oscillations, nonlinear streaming is found to significantly increase the meridional overturning.

1. Introduction

The ideal thermocline equations, which describe the density and momentum balances of a frictionless fluid in geostrophic and hydrostatic balance, form one of the simplest systems

1. Department of Mathematics, Keele University ST5 5BG, United Kingdom.

which can usefully be used to describe global (gyre) scale ocean circulation patterns. These equations, sometimes with the addition of vertical diffusion of density, have therefore formed the basis of most of the analytical work on such flows. Solutions typically take a similarity form which relies on some symmetry property of the equations to reduce the number of independent variables from three to two. Examples include the work of Niiler and Dubbelday (1970), Welander (1971), Young and Ierley (1986) and Killworth (1987). However, Salmon and Hollerbach (1991) were the first to use the group theoretical techniques pioneered by Sophus Lie in the 19th century to systematically catalogue a large class of point symmetries and symmetry solutions to the thermocline equations. These authors utilized what is now normally described as the classical symmetry method.

An alternative strategy for reducing the number of independent variables is to consider a fluid of many homogeneous layers, in which the layer thicknesses become additional dependent variables. This approach was used to great effect in the work of Luyten *et al.* (1983), and by de Szoeke (1995). All of these solutions tend to become unrealistic close to boundaries where diffusive or inertial effects would, in reality, be significant.

The inclusion of additional physical effects, such as horizontal diffusion or linear damping of momentum, can lead to symmetry breaking and thus restrict the possible similarity forms, although Filippov (1968) has derived and examined some such solutions. If, instead, the equations are extended by allowing for the rate of change of density, the classical symmetry method can still produce genuinely new symmetries. These will then, in the first instance, have the effect of reducing the number of independent variables back to three. Such a symmetry can then be expressed in the form of an unknown function of three transformed coordinates, which satisfies some new equation derived from the original equations. In the most interesting case, the derived equation is precisely the time-independent form of the thermocline equations. Thus the symmetry gives a recipe by which any solution of the ideal steady thermocline equations can be used to produce a related solution of the time-dependent equations. In Sections 2 and 3 of this article a symmetry of this type is presented and analyzed; in Section 4 the symmetry is applied to an example steady solution; and in Section 5 more general symmetries are discussed.

We then describe the results of numerical simulations aimed at assessing the extent to which these solutions are relevant to flows with dissipation in bounded domains of global scale. Linear friction is added to the momentum balance so that the equations can satisfy a no normal flow boundary condition at all boundaries; a more realistic equation of state is used, in which density depends linearly on salinity and nonlinearly on temperature; a convective adjustment term is included so that static stability is maintained at every timestep; and diffusion of heat and salt is added to represent subgrid scale mixing and to improve numerical stability. The question of appropriate boundary conditions for the diffusive fluxes in the resulting system is not trivial and is discussed in Section 6, where the numerical model is described, and in the Appendix. In Sections 7 and 8 we describe how the model behaves when the surface forcing functions oscillate with a period of between one and forty years. Finally, in Sections 9 and 10, we make comparisons with the behavior predicted by the analytical solution and summarize our conclusions.

2. Governing equations and the classical symmetry method

The time-dependent ideal thermocline equations can be expressed in the following dimensionless form.

$$\begin{aligned} -fv &= -\phi_x, \\ fu &= -\phi_y, \\ \theta &= \phi_z, \\ u_x + v_y + w_z &= 0, \\ \theta_t + u\theta_x + v\theta_y + w\theta_z &= 0. \end{aligned} \tag{1}$$

Here $\mathbf{u} = (u, v, w)$ is the fluid velocity in a Cartesian coordinate system in which x is directed eastward, y northward and z vertically upward. ϕ is pressure or geopotential while θ represents temperature or (more generally) buoyancy. Subscripts denote differentiation. For convenience, the Coriolis parameter f will subsequently be set to y. For a discussion of the validity of these equations for large-scale ocean flows see for instance Pedlosky (1987).

A brief explanation of how symmetry group methods can be used to derive solutions to differential equations appears in Salmon and Hollerbach (1991). For an authoritative text on the subject the reader is referred to the works by Olver (1986) or Bluman and Kumei (1989). The objective here is merely to present solutions, which can readily be verified to satisfy the appropriate governing equations. It is therefore not appropriate, in this instance, to give more than the following brief overview of the salient points of the technique, with reference to the thermocline equations.

Most importantly for the applied scientist, classical symmetry group methods can be applied to arbitrary nonlinear differential equations in a way which is sufficiently formulaic that most of the analysis can be carried out by readily available algebraic manipulation packages. It is not necessary to have a deep understanding of the underlying group theory to make use of the technique. It is straightforward to analyse sets of equations such as (1), although the thermocline equations can be expressed, without loss of generality, as a single equation for a potential function M. The potential, M, can be defined by a vertical integral of pressure. The equivalent form of (1) is

$$y^2 M_{zzt} + yJ(M_z, M_{zz}) + M_x M_{zzz} = 0, \tag{2}$$

where

$$u = -\frac{1}{y} M_{zy}, \qquad v = \frac{1}{y} M_{zx}, \qquad w = \frac{1}{y^2} M_x, \qquad \phi = M_z, \qquad \theta = M_{zz}. \tag{3}$$

$J(A, B)$ is the Jacobian $A_x B_y - A_y B_x$. It turns out that working with the M equation reveals an additional symmetry, which leads to physically significant solutions despite the fact that the extra symmetry has no dynamical signature (the solution discussed in Section 4 stems from a symmetry of this type). Such symmetries are sometimes referred to as potential symmetries.

In order to find solutions of (2) we first find symmetries of (2). Symmetries are transformations of the dependent and independent variables which leave the thermocline equation (2) unchanged. Solutions of (2) can be written as

$$\Gamma(x, y, z, t, M) = 0, \tag{4}$$

and can be thought of as four-dimensional surfaces in a five-dimensional space. The equation itself,

$$\Delta(x, y, z, t, M, M_x, \ldots, M_{zzz}) = 0, \tag{5}$$

is considered as a hypersurface in a much higher dimensional "jet" space in which each derivative of the dependent variable constitutes an additional dimension. Since symmetries map the equation to itself, they are normally described as finite transformations corresponding to infinitesimal symmetry generators, which at each point define a direction which is tangent to the equation surface defined by (5). Thus the generators lie in a tangent space, and are usually expressed as differential operators (such as $x\partial_x - y\partial_y$). Such an operator, **v** say, acting on the coordinates of the base space (x, y, z, t, M) defines a transformation of coordinates in the jet space. This extended or "prolonged" transformation *pr***v** can be expressed in terms of the components of the base transformation **v**. By equating coefficients in the jet space, the condition that the transformation maps the equation surface to itself then gives rise to a large set of simultaneous differential equations in the elements of **v**. These equations, although usually heavily overdetermined, are nonetheless linear. They can therefore very often be readily solved by simple algorithmic methods. Their solution then gives a very general point symmetry of the original equation. We have used the PC program Mulie written by Alan Head (Head, 1993) to set up and solve these determining equations; several other packages exist which can also perform this task. Mulie runs on IBM type PCs and is available by anonymous ftp on the internet.

These symmetries can be used to generate new solutions from known solutions. For instance, if $M(x, y, z)$ is a steady solution of (2), then $M(\alpha, y, z)$ is also a steady solution for any function $\alpha(x, y)$, as noted by Killworth (1983). This transformation is particularly useful as it can be used to ensure that solutions satisfy a condition of no mass flux through an eastern boundary. A more powerful consequence of the knowledge of the symmetry properties of an equation is that they can be used to find similarity solutions. These are solutions which are unaffected by a given symmetry transformation. In the language of differential operators, such solutions are invariant under a given symmetry generator so that the condition that a solution Γ be invariant, for instance, becomes $\mathbf{v}\Gamma = 0$. For instance, the translational invariance in the x direction, expressed by the function α above, leads to similarity solutions $M = M(y, z)$. Scaling symmetries lead to solutions in which M depends on ratios of the independent variables raised to various powers, for instance the similarity form discovered by Young and Ierley (1986);

$$M = x^{a/(1+a)} G(zx^{-a/(1+a)}, yx^{a/(1+a)}), \tag{6}$$

where G is a function to be determined by substitution into the steady form of (2).

For a given equation the symmetry generators form a Lie algebra and the power of the theory lies in its ability to find an optimal subset of symmetry generators which can be used to obtain all the elements of the algebra, and thus their associated similarity solutions.

Similarity solutions are normally found by solving characteristic equations corresponding to motion along the direction defined by a symmetry generator $\mathbf{v}$. This fixes the solution in the form of an unknown function which satisfies an equation to be derived by substitution into the original equation, and which depends on a smaller number of dependent variables than appeared in the original equation. The process can be repeated until an equation is obtained which is simple enough that explicit solutions can be derived by other means.

Note that the classical method described above may not find all the symmetries of a given equation. More powerful methods such as the direct method of Clarkson and Kruskal (1989) can sometimes find more symmetries but the equations determining the symmetry generators are typically nonlinear with these more general methods and are not always readily solved.

The symmetries of (2) are mostly identical to, or generalizations of, those given by Salmon and Hollerbach for the steady case. The full set of symmetry generators found by the classical method can be written as

$$\begin{aligned}
\mathbf{v}_1 &= \frac{1}{y}\psi_y\partial_x - z\psi_t\partial_M \\
\mathbf{v}_2 &= 2x\partial_x - y\partial_y \\
\mathbf{v}_3 &= \beta(t)\partial_z + xy^2\dot{\beta}(t)\partial_M \\
\mathbf{v}_4 &= x\partial_x + z\partial_z + 2M\partial_M \\
\mathbf{v}_5 &= x\partial_x + M\partial_M \\
\mathbf{v}_6 &= 2\dot{\alpha}(t)x\partial_x - \dot{\alpha}(t)y\partial_y - \dot{\alpha}(t)z\partial_z - (2\dot{\alpha}(t)M + \ddot{\alpha}(t)xy^2z)\partial_M + \alpha(t)\partial_t \\
\mathbf{v}_7 &= z^2\partial_M \\
\mathbf{v}_8 &= \gamma(y, t)\partial_M
\end{aligned} \tag{7}$$

$\alpha(t)$, $\beta(t)$, $\gamma(y, t)$ and $\psi(y, t)$ are arbitrary functions. These correspond closely to the eight generators for the steady thermocline equations listed by Salmon and Hollerbach. $\mathbf{v}_2$, $\mathbf{v}_5$ and $\mathbf{v}_7$ are all unchanged by time-dependence. Scaling in x ($\mathbf{v}_1$) can no longer depend arbitrarily on x and y but may depend on y and t. $\mathbf{v}_3$ and $\mathbf{v}_8$ have been generalized to include arbitrary time-dependence, $\mathbf{v}_4$ differs from the steady counterpart which is simply $x\partial_x + z\partial_z$ while $\mathbf{v}_6$ is the only generator which directly affects the time variation of solutions. The rest of this paper is concerned mostly with a similarity solution which stems from $\mathbf{v}_6$, and is a small generalization of a solution originally found by Rick Salmon (private communication).

To determine the finite symmetry transformation and the similarity solution correspond-

ing to the generator $\mathbf{v}_6$, we solve the characteristic equations

$$\frac{dx}{2\dot{\alpha}x} = \frac{-dy}{\dot{\alpha}y} = \frac{-dz}{\dot{\alpha}z} = \frac{-dM}{2\dot{\alpha}M + \ddot{\alpha}xy^2z} = \frac{dt}{\alpha}. \tag{8}$$

The solution of (8) is that the following quantities are constant

$$x\alpha^{-2}, \qquad y\alpha, \qquad z\alpha, \qquad \alpha^2 M + \dot{\alpha}\alpha xy^2 z. \tag{9}$$

Thus $\mathbf{v}_6$ generates the finite transformation of coordinates

$$(x, y, z, t, M) \mapsto (x\alpha^{-2}, y\alpha, z\alpha, \eta(t), \alpha^2 M + \dot{\alpha}\alpha xy^2 z), \tag{10}$$

for a function $\eta(t)$ which is determined below. This coordinate transformation allows us to generate new solutions from known solutions; if $M_0(x, y, z, t)$ is a solution of (2), then

$$M = \alpha^{-2} M_0(x\alpha^{-2}, y\alpha, z\alpha, \eta(t)) - \frac{\dot{\alpha}}{\alpha} xy^2 z \tag{11}$$

should also be a solution. Substituting into (2) shows that this is indeed the case if $\alpha = 1/\dot{\eta}$.

To find a similarity solution we first write one of the invariants as a function of the others;

$$\alpha^2 M + \dot{\alpha}\alpha xy^2 z = G(x\alpha^{-2}, y\alpha, z\alpha). \tag{12}$$

G depends on only three independent variables (one less than we started with) and satisfies an equation which is found by substituting into (2). In this case the equation turns out to be the time-independent form of (2). (2) has thereby been "solved" in the sense that solutions can now be found in terms of solutions to a simpler equation. This process can of course be repeated until the number of independent variables is reduced to one.

For reference, we now list the finite transformations for all eight of the generators given above.

$$\begin{aligned}
&\mathbf{v}_1 : (x, y, z, t, M) \mapsto \left(x + \frac{1}{y}\psi_y, y, z, t, M - z\psi_t\right)\\
&\mathbf{v}_2 : (x, y, z, t, M) \mapsto (c^2 x, c^{-1} y, z, t, M)\\
&\mathbf{v}_3 : (x, y, z, t, M) \mapsto (x, y, z + \beta(t), t, M + xy^2\dot{\beta}(t))\\
&\mathbf{v}_4 : (x, y, z, t, M) \mapsto (cx, y, cz, t, c^2 M)\\
&\mathbf{v}_5 : (x, y, z, t, M) \mapsto (cx, y, z, t, cM)\\
&\mathbf{v}_6 : (x, y, z, t, M) \mapsto (\dot{\eta}^2 x, \dot{\eta}^{-1} y, \dot{\eta}^{-1} z, \eta(t), \dot{\eta}^{-2} M - \ddot{\eta}\dot{\eta}^{-3} xy^2 z)\\
&\mathbf{v}_7 : (x, y, z, t, M) \mapsto (x, y, z, t, M + cz^2)\\
&\mathbf{v}_8 : (x, y, z, t, M) \mapsto (x, y, z, t, M + \gamma(y, t))
\end{aligned} \tag{13}$$

3. Physical interpretation

If we let M_0 denote any given solution of the steady ideal thermocline equation, we can now write down an associated solution of (2), using $\mathbf{v}_3$ and $\mathbf{v}_6$,

$$M(x, y, z, t) = \alpha^{-2} M_0(\alpha^{-2}x, \alpha y, \alpha z - \beta) + \alpha^{-1} xy^2 \dot{\beta} - \frac{\dot{\alpha}}{\alpha} xy^2 z, \tag{14}$$

where α and β are arbitrary functions of time. Writing $\mathbf{x} = (x, y, z)$ and

$$\mathbf{s} = (\alpha^{-2}x, \alpha y, \alpha z - \beta), \tag{15}$$

the velocity components are

$$\begin{aligned} u(\mathbf{x}, t) &= \alpha u_0(\mathbf{s}) + \frac{2\dot{\alpha}x}{\alpha}, \\ v(\mathbf{x}, t) &= \alpha^{-2} v_0(\mathbf{s}) - \frac{\dot{\alpha}y}{\alpha}, \\ w(\mathbf{x}, t) &= \alpha^{-2} w_0(\mathbf{s}) + \alpha^{-1}\dot{\beta} - \frac{\dot{\alpha}z}{\alpha}, \end{aligned} \tag{16}$$

where the subscript 0 denotes the value of a variable in the steady solution. The pressure is

$$\phi(\mathbf{x}, t) = \alpha^{-1}\phi_0(\mathbf{s}) - \frac{\dot{\alpha}}{\alpha} xy^2 \tag{17}$$

while the temperature θ is simply

$$\theta(\mathbf{x}, t) = \theta_0(\mathbf{s}). \tag{18}$$

It is clear from (18) that this solution has an extremely simple interpretation: contours of θ, i.e. isopycnals, are translated from an initial position $\mathbf{s}$ to $\mathbf{x}$. This translation defines an invertible transformation $\mathbf{x}(\mathbf{s}, t)$, in which case the velocity which advects the isopycnals is $\dot{\mathbf{x}}$, where

$$\dot{\mathbf{x}} = \left(\frac{2\dot{\alpha}x}{\alpha}, -\frac{\dot{\alpha}y}{\alpha}, \alpha^{-1}\dot{\beta} - \frac{\dot{\alpha}z}{\alpha} \right). \tag{19}$$

This is discussed in more detail in Section 5, but note from (19) that the advecting velocity is linear in $\mathbf{x}$. The solution therefore represents linear distortion of isopycnals, although it should be noted that while the advecting velocity is linear in $\mathbf{x}$, the solution itself is nonlinear in α. Nevertheless, (19) will be referred to as the "linear (isopycnal) distortion solution." This time-dependent distortion seems most likely to be physically relevant when the function $\alpha(t)$ is periodic (for instance $\alpha = 1 + \epsilon \sin(\omega t)$) for then, within a bounded domain, the distortion will remain bounded. If $\epsilon \ll 1$ then the advecting velocity $\dot{\mathbf{x}}$ may also stay within realistic limits. Nonperiodic solutions might be applicable to the study of

shock formation. Such solutions would be valid up to a finite time after which diffusive processes became important.

The potential vorticity q in this formulation is $y\theta_z$ which, in the time-dependent solution, becomes

$$q(\mathbf{x}, t) = q_0(s). \tag{20}$$

So the potential vorticity is also simply advected by the velocity $\dot{\mathbf{x}}$. In the steady ideal thermocline equations the three quantities θ, q and the Bernoulli function B are all constant on streamlines ($B = \phi - \theta z$ or in terms of M, $M_z - zM_{zz}$); hence any one can be expressed as a function of the other two. Killworth (1987) exploits this fact to derive some of the most realistic similarity solutions of the ideal equations. These similarity solutions arise from basic scaling symmetries but they only become linear, and thus tractable, when expressed in density coordinates. The assumed similarity form requires that

$$qB = F(\rho), \tag{21}$$

where ρ is density, which is equivalent to $-\theta$ in our notation. This relationship was introduced by Welander (1971) and is also satisfied by the layered solutions of Luyten *et al.* (1983). Some of the similarity forms of Salmon and Hollerbach (1991) could be expressed in this form, but only with F a complicated differential function of ρ. For the present solution (14), if $\beta = 0$, B is

$$B(\mathbf{x}, t) = \alpha^{-1}B_0(\mathrm{s}) - \frac{\dot{\alpha}}{\alpha}xy^2, \tag{22}$$

thus qB is not in general a function only of ρ while $\dot{\alpha}$ is nonzero. However if $\dot{\alpha}$ returns to zero at some time, so that one steady solution has been distorted into another, and if the original solution satisfies (21), the new solution satisfies

$$\begin{aligned} q(\mathbf{x})B(\mathbf{x}) &= \alpha^{-1}q_0(\mathbf{s})B_0(\mathbf{s}) \\ &= \alpha^{-1}\mathrm{F}(\rho_0(\mathbf{s})), \end{aligned} \tag{23}$$

so the similarity form is preserved up to a constant scaling factor. Note that in density coordinates (x, y, ρ) with $f = y$, the time dependent B equation is $B_{\rho\rho t} + J(B, B_{\rho\rho}/y) = 0$, which has the symmetry solution

$$B = \frac{c}{\alpha}B_0(a\alpha^{-2}x, \alpha y, \rho) - \frac{\dot{\alpha}}{\alpha}xy^2, \tag{24}$$

where a and c are arbitrary constants, $\alpha(t)$ is arbitrary and B_0 is a steady solution. This is almost equivalent to (22) except that the distortion remains on density surfaces.

Similarity solutions are notoriously bad at satisfying realistic boundary conditions. In fact, even the thermocline equations in general can only satisfy very limited conditions at boundaries. Typically the philosophy for similarity solutions is to attempt to satisfy no normal flow through the bottom and eastern boundaries, and to impose surface distribu-

tions of density (or temperature) and vertical velocity (representing an Ekman pumping out of an unresolved mixed layer). Often there is limited freedom with respect to the surface conditions, and the forms of the surface fields are part of the solution.

Because the time-dependent M equation (2) inherits the symmetry generators corresponding to translation in z and, in an only slightly restricted form, in x, the solution (14) can be made to satisfy similar boundary conditions to the steady solution M_0. In particular, we can assume without loss of generality that the bottom and eastern boundaries lie at $z = 0$ and $x = 0$ respectively, whereby it is clear from Eq. (19) that if $\beta = 0$, the linear distortion solution (14) does not advect points across these boundaries. Thus if $\mathbf{u}_0.\mathbf{n} = 0$ on these boundaries in the steady solution, where $\mathbf{n}$ is a vector normal to the boundary, then the same holds for the time-dependent solution (but see below for a caveat to this). The β term simply corresponds to a change of origin in z and will henceforth be ignored. If the surface in the scaled coordinates lies at $z = 1$ then Eqs. (18) and (16) state that the temperature and vertical velocity there are

$$\theta(x, y, 1, t) = \theta_0(\alpha^{-2}x, \alpha y, \alpha), \tag{25}$$

$$w(x, y, 1, t) = \alpha^{-2}w_0(\alpha^{-2}x, \alpha y, \alpha) - \frac{\dot{\alpha}}{\alpha}\cdot \tag{26}$$

Compared to the steady solution, there is an extra component to the vertical velocity, a rearrangement of the surface values and a change due to vertical distortion (that is, values at $z = 1$ at time t correspond to values at $z = \alpha(t)$ in the steady solution). If $\alpha = 1 + \epsilon \sin(\omega t)$ as proposed earlier, these changes constitute small oscillations of the surface forcing functions about their steady values.

One other possibility is to consider the solution scaled such that the isopycnal distortion has no surface signature, for instance by defining the surface to be the origin of z. This might represent slow modulation of a large-scale flow pattern by time-dependent upwelling from abyssal to thermocline waters.

Because the advecting velocity $\dot{\mathbf{x}}$ is necessarily linear in $\mathbf{x}$, the linear distortion solution does not fit into the traditional framework for the analysis of stability of steady solutions to small spatially periodic perturbations. Further, if we choose the advecting velocity to be zero at $z = 0$ then the time-dependence is intimately related to changes in the surface forcing. Whether the solution could be used to demonstrate the existence of an energetically favorable departure from a known steady solution depends on the details of the steady solution. One aspect of this question concerns the origin of the changes in internal energy which occur; this is determined for a particular example in the following section.

The vulnerability of a given solution to arbitrary disturbances will in general be affected by the distortion process. There may not be a great qualitative change because both the temperature and potential vorticity fields are advected without interior topological changes. For instance Killworth (1987) notes that in his type I solutions q_y changes sign in the domain, suggesting the susceptibility of the solution to eddying and consequent potential vorticity homogenization in the southern half of the gyre. The simple advection of q

contours by the linear distortion solution means the same remarks apply to any such distortion of these solutions. Following Charney and Stern (1962), Pedlosky (1987) derives a necessary condition for instability and shows that if q_y does not change sign within the domain, then one of two other conditions must hold. Either the product of q_y and θ_y should be positive somewhere on the upper boundary, or else a similar condition applies involving the meridional slope of θ surfaces minus the meridional slope of the lower boundary. In principle the condition at the upper boundary could be affected by the advection of isopycnal surfaces from below, however, only the condition at the lower boundary seems likely to be affected qualitatively by the linear distortion process, if the distortion reverses the relative magnitudes of the slope of the boundary and the slope of θ surfaces.

4. An example

In order to work out the energy transfers implied by the linear distortion solution (14), it is necessary to consider an example steady solution M_0. The time-dependent extension might then represent, for instance, seasonal variation of the steady state. The solution to be used is one of those discussed by Salmon and Hollerbach (1991); their Eq. (8.12). The ocean is taken to occupy the region $0 \le x \le 1, 0 \le z \le 1, 0 < y_S \le y \le y_N$. With the time-dependent extension (14) translated so as to satisfy no normal flow at $x = 1$, and with β set to zero, the solution becomes

$$\begin{aligned}
u &= \frac{2w_E}{\alpha h_0}(2\alpha z - z_0)(1 - x) + \frac{C}{2\alpha^2 y^3}\Big[(\alpha z - z_0)^2 H(\alpha z - z_0) \\
&\quad - \frac{1}{3}h_0^2(2\alpha z - z_0)\Big] + \frac{2\dot{\alpha}}{\alpha}(x - 1), \\
v &= \frac{yw_E}{\alpha h_0}(2\alpha z - z_0) - \frac{\dot{\alpha}}{\alpha}y, \\
w &= \frac{w_E}{\alpha h_0}(\alpha z^2 - z_0 z) - \frac{\dot{\alpha}}{\alpha}z, \\
\theta &= -\frac{2y^2 w_E}{h_0}(1 - x) + \frac{C}{\alpha y}\left[(\alpha z - z_0)H(\alpha z - z_0) - \frac{1}{3}h_0^2\right].
\end{aligned} \tag{27}$$

The potential function is

$$\begin{aligned}
M &= -\frac{w_E}{\alpha h_0}(1 - x)y^2(\alpha z^2 - z_0 z) \\
&\quad + \frac{C}{2\alpha^3 y}\left[\frac{(\alpha z - z_0)^3}{3}H(\alpha z - z_0) - \frac{\alpha h_0^2}{3}(\alpha z^2 - z_0 z)\right] \\
&\quad - \frac{\dot{\alpha}}{\alpha}(x - 1)y^2 z.
\end{aligned} \tag{28}$$

Setting $\alpha \equiv 1$ recovers the original solution. In the above, w_E is the vertical velocity at the upper boundary in the steady solution, which is assumed to be constant here, but can in general vary in y without destroying the basic symmetry; z_0 is a constant vertical level at which the potential vorticity in the steady solution jumps from zero below to the value C in the upper layer (the temperature gradient θ_z also jumps at z_0 from zero to a nonzero value); $h_0 = 1 - z_0$; and H is the Heaviside function, which takes the value zero for negative argument and one for positive argument. y needs to be bounded away from the equator ($y = 0$) because of the breakdown of geostrophy there. In the time-dependent solution the velocity at the upper boundary is

$$\frac{w_E h_\alpha}{h_0} - \frac{\dot{\alpha}}{\alpha},$$

where $h_\alpha = 1 - z_0/\alpha$, which is the depth of the interface between the two layers when $\alpha \neq 1$.

If $w_E < 0$ the solution resembles in some aspects the southern part of a subtropical gyre. The w_E terms have no associated vertical temperature gradient and can be thought of as the wind-driven part of the circulation, while the C terms, which have no associated vertical velocity and are therefore independent of the Ekman pumping velocity at the upper boundary, can be thought of as the thermohaline part of the circulation. Upwelling in the lower half of the lower layer drives a poleward flow at depth, while further up the wind-driven flow is southward and eastward. The thermohaline terms add a component to the eastward thermal wind which varies in sign with z. The surface temperature increases to the northwest as a result of the w_E terms and to the south as a result of the C terms. Figure 1 shows the surface temperature and velocity defined by (27) for $\alpha = 1 + \epsilon_0 \cos(2\pi t/P)$ at four different times.

In the steady case the solution can be generalized to a continuous solution of the full thermocline equations with vertical diffusion of temperature, in which case the discontinuity at z_0, which crudely represents the ocean thermocline, is replaced by a smooth change in gradients. The similarity form leads to a linear advection diffusion equation for temperature or potential vorticity in the $y - z$ plane. Vertical distortion in the time-dependent solution means that the similarity solution (14) breaks down if a constant vertical diffusivity is included.

In the steady solution, the thermohaline terms do not contribute to the vertically averaged mass transport and the depth average of the eastward velocity is zero at $x = 1$. This is not the case for the time-dependent solution in which the vertically integrated eastward velocity at $x = 1$ is

$$\frac{Ch_\alpha}{6\alpha y^3}(\alpha h_\alpha^2 - h_0^2). \tag{29}$$

The vertically integrated heat flux through the eastern boundary is not zero even if $\alpha \equiv 1$.

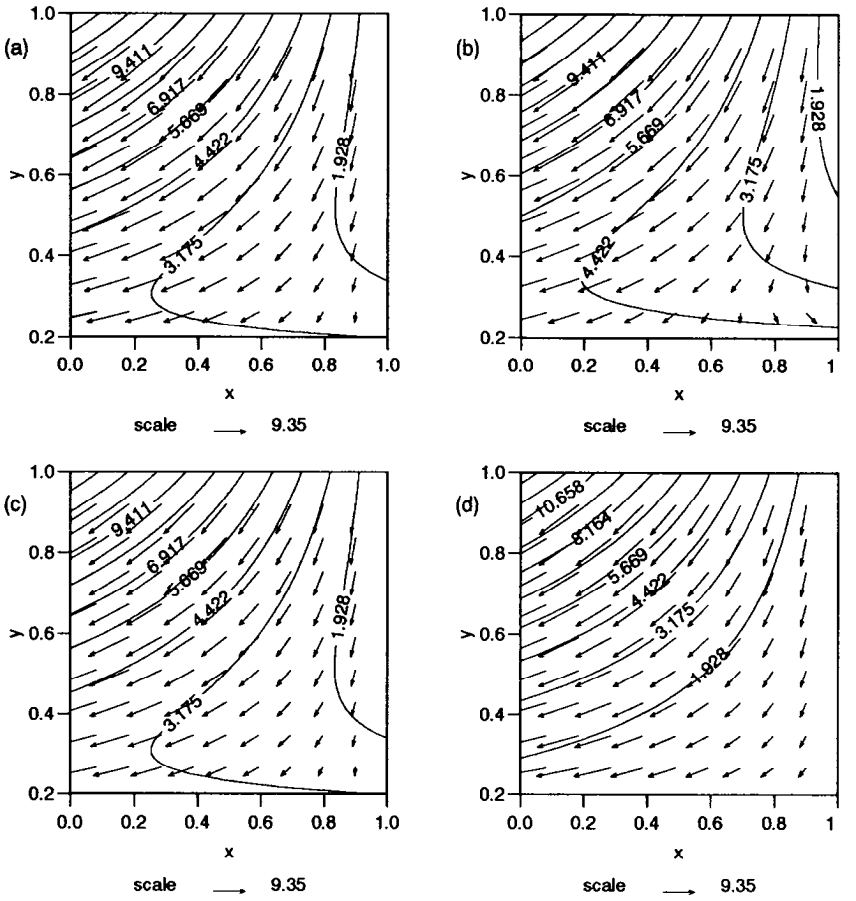

Figure 1. Contours of θ and velocity arrows for the solution (27) at the surface $z = 1$ with $\alpha = 1 + \epsilon_0 \cos(2\pi t/P)$ at times; (a) $t = P/4$, (b) $t = P/2$, (c) $t = 3P/4$, (d) $t = P$. The dimensionless parameters used were; $w_E = -1$, $z_0 = 6/7$, $C = 5$, $P = 1$, $\epsilon_0 = 0.1$.

In the time-dependent solution the net heat flux is

$$\frac{C^2}{2y^4}\left[\frac{h_\alpha^4}{4} + \frac{1}{9\alpha}\left(\frac{1}{\alpha} h_0^4 h_\alpha - h_0^2 h_\alpha^3\right) - \frac{1}{18} h_0^2 h_\alpha^2 (h_\alpha + 3)\right] \tag{30}$$

which reduces to

$$\frac{C^2 h_0^3}{72y^4}(7h_0 - 6) \tag{31}$$

in the steady case.

The fundamental nonlinearity in α of the solution (14) becomes relevant at this point. Assume from here onward that

$$\alpha = 1 + \epsilon(t), \tag{32}$$

where ϵ is a small periodic perturbation whose time-average $\overline{\epsilon(t)}$ is zero. The time-averages of any terms which appear nonlinearly in α will not in general be equal to their values in the steady solution. Hence an exactly periodic distortion of isopycnals by a velocity which is linear in $\mathbf{x}$, represented by (14), will lead to changes in the time-averages of mass and heat fluxes. This can be described as a form of nonlinear streaming associated with the oscillations. If $|\epsilon| < 1$ then $1/(1 + \epsilon) > 1 - \epsilon$, therefore by (32), $\overline{\alpha^{-1}} > 1$. Hence, from (27), the oscillation of the wind-driven part of the solution leads in this case to an additional contribution to the time-averaged mass flux in all three directions. The additional flux, which is a result of the oscillation in the thermocline depth, is of order ϵ^2 and is directed downward and south-westward. There is also a time-averaged flux in the x direction, arising from the thermohaline terms, which is the average of (29). This will be positive for small ϵ, so the sign of the net flux in the x direction will depend on the relative magnitudes of the wind and thermohaline-driven circulations.

From the time-dependent ideal thermocline equations (1) we can derive the energy equation

$$\mathbf{u}.\nabla\phi = w\theta. \tag{33}$$

Since there is no kinetic energy, (33) represents an instantaneous conversion of work done by the pressure field into potential energy, for which the rate equation is

$$\frac{\partial}{\partial t}(-z\theta) = \nabla.(\mathbf{u}z\theta) - w\theta. \tag{34}$$

Thus the integrated form of the equation for the potential energy in a volume V is

$$\frac{d}{dt}\int_V -z\theta \, dV = \oint_{\partial V} (z\theta - \phi)\mathbf{u}.\mathbf{n} \, dS, \tag{35}$$

where $\mathbf{n}$ is the outward pointing normal to the volume V. The energy flux $z\theta - \phi$ is given by

$$z\theta - \phi = -\frac{y^2 w_E z_0}{\alpha h_0}(1 - x) + \frac{C}{2\alpha y}\left[\left(\alpha z^2 - \frac{z_0^2}{\alpha}\right)H(\alpha z - z_0) - \frac{h_0^2}{3\alpha} z_0\right] + \frac{\dot{\alpha}}{\alpha}(x - 1)y^2, \tag{36}$$

and hence

$$\frac{d}{dt}\int_V - z\theta \, dV = -\frac{C\dot{\alpha}}{2\alpha^2} \ln\left(\frac{y_N}{y_S}\right)\left[z_0\left(1 - \left(\frac{z_0}{\alpha}\right)^2\right) + \frac{1}{3}h_0^2\right]. \tag{37}$$

The expressions for the flux of energy into the domain from each of the boundaries (except

the lower boundary where $w = 0$) contain a variety of terms arising from the modulation of the fluxes in the steady solution, as well as additional fluxes whose origin is the advecting velocity in the time-dependent solution. Many of these terms balance separately, so perhaps the most interesting question is to determine the source of the flux which balances the change of energy in the interior (37). The most physically sensible scenario might be that the interior energy change is balanced by the flux of energy at the surface, representing the time varying forcing, but this is not the case. Since the function α remains arbitrary, we can look for terms in the boundary fluxes which have the same functionality in α as (37). It transpires that such terms occur only at the western boundary. They represent work done by the fluctuating ($\dot{\alpha}$) term in the pressure field and fluxes of both kinetic and potential energy due to the advecting velocity $\dot{\mathbf{x}}$. The latter, which correspond to the $\dot{\alpha}\alpha^{-4}$ terms in (37), are a result of the displacement of the "thermocline" to the position z_0/α.

The wind forced part of the solution is only affected by the linear distortion symmetry in a limited way, and does not contribute to the internal energy change. The fact that the change of interior energy in this solution is due to fluxes from the western boundary implies that these are the only unbalanced energy fluxes which result directly from the distortion. They will not generally be the largest. Neither is it clear to what extent this balance is a result of the choice of steady solution M_0.

5. More general advection symmetries

The linear distortion solution (14) is a special case of a far more general symmetry which applies to the advection equation for a passive scalar χ (note that density is not passive in the thermocline equations as it affects the velocity field). If there is a steady state χ_0 and a steady velocity field $\mathbf{u}_0$ such that

$$\mathbf{u}_0.\nabla\chi_0 = 0, \tag{38}$$

then any invertible transformation $\mathbf{s} \mapsto \mathbf{x}(\mathbf{s}, t)$ defines a solution of the time-dependent advection equation

$$\frac{\partial\chi}{\partial t} + \mathbf{u}.\nabla\chi = 0, \tag{39}$$

where

$$\begin{aligned} \chi(\mathbf{x}, t) &= \chi_0(\mathbf{s}), \\ u_i(\mathbf{x}, t) &= \frac{\partial x_i}{\partial s_j} u_{0j}(\mathbf{s}) + \dot{x}_i(\mathbf{s}, t). \end{aligned} \tag{40}$$

This is not difficult to verify using the chain rule:

$$\frac{\partial\chi}{\partial x_i} = \frac{\partial s_j}{\partial x_i}\frac{\partial\chi_0}{\partial s_j}\bigg|_s. \tag{41}$$

The advecting velocity $\dot{\mathbf{x}}$ can then distort the contours of χ_0 in an arbitrary (non-singular) way. Restrictions on the form of $\dot{\mathbf{x}}$ come about in the case of a non-passive scalar due to the relationship between χ and $\mathbf{u}$. For the thermocline equations the thermal wind relations must be satisfied. For a general transformation, these take the form

$$y\epsilon_{3ij}\frac{\partial}{\partial z}\left(\frac{\partial x_j}{\partial s_k}u_{0k}(\mathbf{s}) + \dot{x}_j\right) = \frac{\partial s_k}{\partial x_i}\frac{\partial \theta_0}{\partial s_k}. \tag{42}$$

Apparently these can only be satisfied if the transformation matrix $\partial s_k/\partial x_i$ is diagonal, in which case the advecting velocity has no thermal wind signature (it must also be divergence free). Although the fact that a solution exists at all appears to rely on the special form of the Coriolis parameter (i.e. the beta plane assumption), it is easy to show that a symmetry of exactly the same form as (14) also exists in global spherical polar coordinates, where the Coriolis parameter can again be used as the latitudinal coordinate.

Ertel's potential vorticity provides a further example to show that the increased generality of Eqs. (38) to (41) is more than merely an aid to understanding, although the advecting velocity must again be linear and the temperature can only vary in z. Suppose that there exists a steady velocity field $\mathbf{u}_0$ and steady temperature and density distributions θ_0 and ρ_0 so that the potential vorticity P_0 is

$$P_0 = \frac{\nabla \times \mathbf{u}_0 + 2\Omega}{\rho_0}\frac{\partial \theta_0}{\partial z}, \tag{43}$$

and that $\mathbf{u}_0.\nabla P_0 = 0$. Then if $\mathbf{s} = (\alpha x, \alpha y, c\alpha^{-2}z)$, where the constant c and the function $\alpha(t)$ are arbitrary, it is easy to show that if

$$\begin{aligned}
P(\mathbf{x}, t) &= P_0(\mathbf{s}),\\
\theta(\mathbf{x}, t) &= \frac{\alpha^2}{c}\theta_0(\mathbf{s}),\\
u(\mathbf{x}, t) &= \alpha^{-1}u_0(\mathbf{s}) - \frac{\dot{\alpha}x}{\alpha},\\
v(\mathbf{x}, t) &= \alpha^{-1}v_0(\mathbf{s}) - \frac{\dot{\alpha}y}{\alpha},\\
w(\mathbf{x}, t) &= \frac{\alpha^2}{c}w_0(\mathbf{s}) + \frac{2\dot{\alpha}z}{\alpha},\\
\rho(\mathbf{x}, t) &= \rho_0(\mathbf{s}),
\end{aligned}$$

then $\mathbf{u}$ is also divergence free and P satisfies

$$\frac{\partial P}{\partial t} + \mathbf{u}.\nabla P = 0. \tag{44}$$

One other important symmetry property of the time-dependent thermocline equations deserves to be pointed out. The fact that fairly general translations in x are still permitted in the time-dependent form, as a result of the symmetry generator $\mathbf{v}_1$, means that completely general steady solutions can be converted to wave solutions travelling in the x direction. The transformation of solutions generated by the symmetry $\mathbf{v}_1$ can be expressed in the form

$$M = M_0\left(x - \frac{1}{y}\psi_y, y, z\right) - z\psi_t, \tag{45}$$

where the propagation speed of the disturbance in the x direction is

$$-\frac{1}{y}\psi_{yt}$$

and M_0 is a solution of the steady ideal thermocline equation. The steady solution therefore propagates with a barotropic velocity which depends arbitrarily on y and t. v, w, θ and q are advected with M but an extra velocity component in the propagation direction appears, so that u becomes

$$u = u_0 - c + \left(\frac{1}{y}\psi_y\right)_y v_0.$$

6. The numerical model and the basic steady solution

By constructing a numerical model with more complete dynamics, we can overcome some of the problems associated with boundary conditions which limit the validity of the analytical solutions. Our aim is to consider the extent to which the qualitative features of the linear isopycnal distortion similarity solution can be reproduced by such a model.

To this end we take as starting point the thermocline equations with the addition of a linear drag in the horizontal momentum equations. A more general equation of state is allowed for, with separate equations for salinity S and temperature T, both of which are subject to horizontal and vertical diffusion as well as convective adjustment.

Referred to spherical polar coordinates (ϕ, s, z), where ϕ is longitude, $s = \sin\theta$, θ is latitude and z is measured vertically upward, the equations can be expressed in the dimensionless form

$$-sv = -\frac{1}{c}\frac{\partial p}{\partial \phi} - \lambda u + \frac{\partial}{\partial z}\tau^{\phi}, \tag{46}$$

$$su = -c\frac{\partial p}{\partial s} - \lambda v + \frac{\partial}{\partial z}\tau^{s}, \tag{47}$$

$$\frac{\partial p}{\partial z} = -\rho, \tag{48}$$

$$\frac{\partial}{\partial \phi}\left(\frac{u}{c}\right) + \frac{\partial}{\partial s}(vc) + \frac{\partial w}{\partial z} = 0, \tag{49}$$

$$\rho = \rho(S, T), \tag{50}$$

$$\frac{D}{Dt}X = \kappa_H\left[\frac{\partial}{\partial \phi}\left(\frac{1}{c^2}\frac{\partial X}{\partial \phi}\right) + \frac{\partial}{\partial s}\left(c^2\frac{\partial X}{\partial s}\right)\right] + \kappa_V\frac{\partial^2 X}{\partial z^2} + \mathscr{C}. \tag{51}$$

In the above, $c = \cos\theta$, λ is the drag coefficient and $\boldsymbol{\tau} = (\tau^\phi, \tau^s)$ is the (dimensionless) wind stress. Horizontal lengths have been scaled by the Earth's radius r_0; vertical lengths by a typical mid-ocean depth D; the horizontal velocity components (u, v) in the (ϕ, s) directions have been scaled by a typical horizontal velocity U; and the vertical velocity w has been scaled by UD/r_0. The scalings for the perturbation pressure p and density ρ are derived from the geostrophic and hydrostatic relations respectively. Quantity X in (51) represents either temperature T or salinity S and

$$\frac{DX}{Dt} = \frac{\partial X}{\partial t} + \frac{\partial}{\partial \phi}\left(\frac{uX}{c}\right) + \frac{\partial}{\partial s}(vcX) + \frac{\partial}{\partial z}(wX) \tag{52}$$

is the material derivative. Scalings for salt S and temperature T are not necessary because they appear linearly in Eq. (51); their magnitudes depend on the boundary forcing. The time scale is r_0/U. $\mathscr{C}$ is the convective adjustment term, which acts to remove static instability while conserving S and T. The convection scheme renders each fluid column completely stable at every timestep by iteratively searching for instability and combining adjacent levels into vertically uniform regions. Combining two levels in this way may cause the new region to be unstable with respect to the levels immediately above or below, but since the size of the homogeneous region increases by one vertical level each time instability is detected, it is possible to ensure complete mixing in a small finite number of steps (Rahmstorf, 1993). The state equation for the dimensional density ρ_* takes the form

$$\rho_* = 1000 + 0.7968S - 0.0559T - 0.0063T^2 + 3.7315 \times 10^{-5}T^3, \tag{53}$$

which closely approximates the UNESCO formula for observed ocean density in kgm^{-3} if S is in practical salinity units and T in degrees Celsius (Gill, 1982). In this and several other respects we follow Winton and Sarachik (1993), who used a similar model to study long period oscillations of the thermohaline circulation which can occur with increased surface salinity forcing.

These equations can satisfy a boundary condition of no normal flow at all boundaries, but beyond that, clarity in respect of the appropriate boundary conditions has hitherto been lacking. The no normal flow condition implies a mixed condition on the derivatives of ρ at the boundary which makes it impractical to specify the gradients of T and S. However, by postulating a distribution of diffusivity κ_H which tends to zero at the lateral boundaries, it is possible to see how specifying no diffusive flux across these boundaries may result in a well posed mathematical problem. This point is discussed in depth in the Appendix.

The equations are solved in a 60° wide sector of uniform depth D from 10° to 70° North, using surface forcing functions which were found by Winton and Sarachik to result in a stable steady circulation. Thus the heat flux out of the top grid box is given by

$$-\kappa_V \frac{\partial T}{\partial z} = -\frac{T_a - T_o}{\tau_r} \Delta z, \tag{54}$$

where Δz is the depth of the top grid level, T_o is the temperature in the top grid level, τ_r is a restoring timescale, and the prescribed atmospheric temperature T_a is

$$T_a = A \cos (c_1(\theta - \theta_0)),$$

where A, c_1 and θ_0 are constants. The wind stress is purely zonal with amplitude

$$\tau^\phi = B \cos (c_2(\theta - \pi/4)) + C,$$

and the surface salinity flux is derived from the gradient of an implied steady state northward flux of salinity F through the basin given by

$$F = \frac{D}{\cos \theta} \sin \left(\frac{\pi(\theta - \theta_0)}{\theta_1 - \theta_0} \right).$$

B, C, D, c_2 and θ_1 are constants. The use of mixed surface boundary conditions, in which the salinity flux is fixed but the heat flux is variable, is an approximation which has been shown to affect the stability of steady solutions (Zhang *et al.,* 1993; Rahmstorf and Willebrand, 1995; Cai, 1995). The form of the surface boundary conditions does not have a strong effect on our solutions. Diffusion parameter values have been chosen to ensure numerical stability, while the Rayleigh friction parameter λ in the momentum equation is constrained by the need to have at least one gridpoint in the frictional boundary layers. The values of all the above parameters and their dimensional equivalents, where appropriate, are given in Table 1.

To solve the elliptic problem for the barotropic stream function we use Gaussian elimination, which is time consuming on the first step but extremely fast thereafter (without topography the equation need only be solved once). The velocities can then be found by an integration in z, and the solution advanced to the next time step, after applying convective adjustment. Spatial gradients, which are second order throughout, are expressed in a difference form such that internal heat and salt fluxes are conserved to numerical accuracy throughout the integration. An explicit first order difference scheme is used for timestepping. More than adequate temporal resolution is guaranteed by the small timestep which is necessary to maintain stability. Hence a higher order temporal scheme would be inappropriate. The numerical grid has 20 equally spaced points in each of the s and ϕ directions and 16 logarithmically spaced vertical levels whose separation increases by a factor of ten from top to bottom. To test the model we have repeated the published experiments of Salmon (1990) and Winton and Sarachik (1993) to determine steady states

Table 1. Parameter values, the salt flux equates to a freshwater flux of 1.2 m yr^{-1} at 35 psu at the northern boundary.

Parameter	Value	Dimensional equivalent
A	25	25°C
c_1	1.565	—
θ_0	10°	—
θ_1	70°	—
B	2.400×10^{-3}	0.07 Nm^{-2}
C	1.029×10^{-3}	0.03 Nm^{-2}
c_2	5.143	—
D	5.064×10^{-3}	6.452×10^6 psu m^3 s^{-1}
λ	6.349×10^{-2}	$(1.25 \text{ days})^{-1}$
κ_H	0.01	3185 m^2 s^{-1}
κ_V	1.593×10^{-3}	2×10^{-4} m^2 s^{-1}
τ_r	4.137×10^{-2}	61 days

of the system. The results were sufficiently close to validate the model, in spite of differences in the dynamics and numerical methods.

Our intention is to compare the predictions made by the analytical work of how time-dependent forcing affects steady solutions, with how time-dependence affects steady numerical solutions. Therefore the steady solution corresponding to M_0 to be used for the numerical experiments will be one produced by the numerical model itself. To attempt to use an existing analytical solution instead would make the results harder to interpret. The numerical model will readily produce steady solutions which satisfy appropriate boundary conditions and resemble real ocean flows, although they do not conform exactly to ideal dynamics. In particular numerical solutions include frictional boundary layers.

To produce a steady solution the model is integrated in time from an initially uniform, motionless state for a period of about 2000 years. By this time changes in temperature and salinity are at the level of numerical noise and the residual surface heat flux is 5×10^{-3} Wm^{-2}. The final steady solution is similar to that described in detail by Colin de Verdière (1988, 1989); thermal forcing acts to create an anticyclonic gyre at upper levels, which tends to override the wind driving in the north. Strong sinking occurs in the northeast corner, where convection is required to balance the heat equation. Away from the northern convection region a thermocline develops with a maximum averaged upwelling at about one seventh of the ocean depth. Below the thermocline, advection dominates the budgets of heat and salt except near the northern boundary, and the sense of the circulation is opposite to that in the upper levels, with a southward flowing western boundary current forming one branch of a cyclonic gyre. These qualitative features are stable to variations of drag and diffusion parameters. With the present values we obtain a maximum in the meridional overturning stream function of 17 Sv, and a maximum northward heat flux of 0.8×10^{15} W. Figure 2 shows temperature and velocity on various horizontal and vertical sections through the model domain.

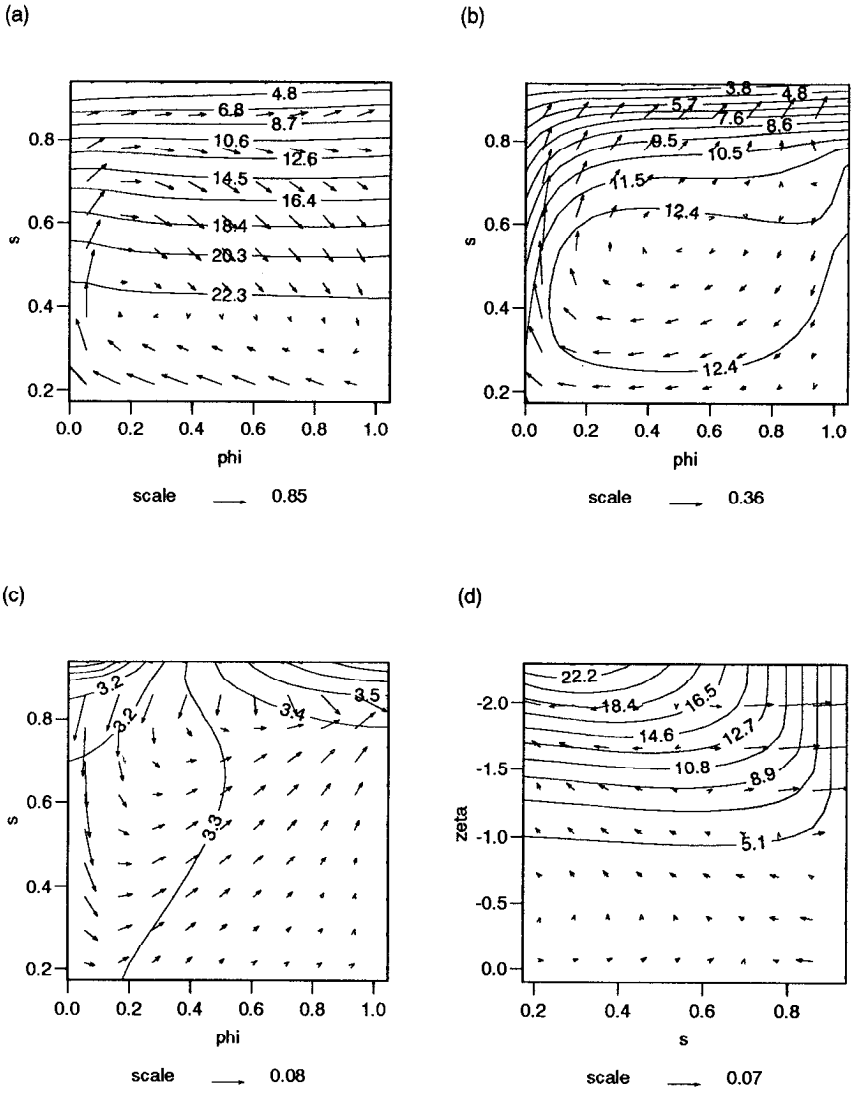

Figure 2. Contours of T and velocity arrows for the numerically generated steady solution; (a) at the surface $z = 1$, (b) upper thermocline $z = 0.9$, (c) near the bottom $z = 0.1$, (d) vertical meridional section at mid-basin $\phi = \pi/6$. Model vertical levels are uniformly spaced in the logarithmic coordinate $\zeta = \log(1 - z + 0.1)$.

7. Numerical experiments with oscillatory forcing

The numerical model is forced by a wind stress and thermohaline fluxes applied over the uppermost grid level, which therefore represents the Ekman mixed layer. These forcings are varied in a way which is consistent with reproducing the time-dependence of the temperature and vertical velocity fields at the base of the Ekman mixed layer as predicted

by the analytical solution. In order to do this we make a number of simplifying assumptions. We first fix the function α by setting

$$\alpha \equiv 1 - \epsilon(t) \equiv 1 - \epsilon_0 \cos(2\pi t/P),$$

and choosing values for the amplitude ϵ_0 and period P. In the analytical solution ϵ_0 is the vertical displacement amplitude. The temperature at the top of the analytical solution, which we take to be the level z_E at the base of the mixed layer, should vary as a result of advection in all three directions. The amplitude of the temperature oscillation is therefore a function of position. We approximate the predicted amplitude by neglecting variation in the north-south direction in favor of vertical variation, which should be dominant in the majority of the domain. For a given amplitude of vertical displacement ϵ_0, we can infer a temperature perturbation to the steady numerical solution by interpolating between the temperature values at the top two gridpoints. We then assume that the surface restoring temperature, which is used to calculate the surface heat flux, varies by the same amount. This is reasonable because the restoring time scale inherent in the temperature boundary condition is 61 days, which is significantly smaller than the oscillation periods to be used in most cases. Values are averaged in the east-west direction, so that the forcing remains zonal, and hence neither encourages nor precludes advection in the zonal direction. In effect we are assuming that close to the surface $z = 1$ the temperature obeys

$$T(z, t) = T_0(\alpha z) = T_0(z) - \epsilon \frac{\partial T_0}{\partial z}, \tag{55}$$

and that the surface restoring temperature T_a is then given by

$$T_a(t) = T_{a0} - \epsilon \left.\frac{\partial T_0}{\partial z}\right|_{z=1}. \tag{56}$$

The subscript zero again denotes the steady solution. It turns out that the required perturbation to the surface restoring temperatures is well fitted by a piecewise linear function of s which is zero over the northernmost quarter of the range of s, and increases to a maximum at the southern boundary.

Two mechanisms contribute to the variation of the vertical velocity at a fixed point in the linear distortion solution (14), namely gradients in the advected steady state vertical velocity w_0, and the additional velocity $\dot{\mathbf{x}}$ corresponding to the distortion itself. Under certain conditions, which are considered later, the latter is dominant. We therefore consider only the additional velocity $-\dot{\alpha}z/\alpha$, the last term in the third equation of (16). To calculate the additional wind stress needed to create this velocity we use the Ekman pumping condition

$$w_E = \mathbf{k}.\nabla \times \left(\frac{\boldsymbol{\tau}}{s}\right). \tag{57}$$

Thus we require an additional eastward wind stress τ^+, which if chosen to be zero at the equator and at the northern boundary s_1, is given by

$$\tau^+ = \frac{\dot{\alpha}}{\alpha}(s - s_1)\frac{s}{c}. \tag{58}$$

Since ϵ will be small it is sufficient to use $\dot{\alpha}$ in place of α/α.

The magnitudes of the changes in w_E due respectively to advection of gradients in the steady state and the distortion velocity $\dot{\mathbf{x}}$ itself can be estimated as

$$\epsilon_0 \frac{\partial w_0}{\partial z} \quad \text{and} \quad \frac{2\pi\epsilon_0}{P}.$$

Thus the latter will be greater for periods P smaller than

$$P_a = 2\pi\left|\frac{\partial w_0}{\partial z}\right|^{-1}. \tag{59}$$

Immediately below the mixed layer at the center of the subtropical gyre in the steady solution the value of P_a is 21.5 or about 80 years. The solutions considered have periods less than 10, so the retained term is indeed more significant in these cases. A measure of the expected relative importance of the thermal forcing can be gained by examining the vertical velocity gradient in an alternative steady solution in which the flow is purely thermohaline driven, that is the wind forcing is set to zero. For a vertical displacement of the same amplitude, the expected change in the vertical velocity w_T at z_E would be approximately

$$\epsilon_0 \frac{\partial w_T}{\partial z}.$$

At the same position below the mixed layer we find the value of $\partial w/\partial z$ is only a factor of two smaller in the thermally driven case than with wind and thermal forcing. This suggests that the thermal forcing is likely to have a similar effect to the advection of vertical velocity gradients, regardless of the amplitude and period of the oscillation. Our neglect of the latter effect may reduce the extent to which our solutions resemble the analytical predictions for the longer period oscillations.

Three different cases will be described, with periods of approximately one, eight and forty years. The amplitudes have been deliberately chosen to be fairly large, to illustrate the effects of the oscillations. Results are shown after 200 to 400 years integration, starting from the steady state, by which time the oscillations have become almost uniformly periodic.

8. Numerical results

a. Rapid oscillations. With an oscillation period of one year, and a dimensionless displacement amplitude ϵ_0 equal to 0.001, the maximum value of the applied wind stress

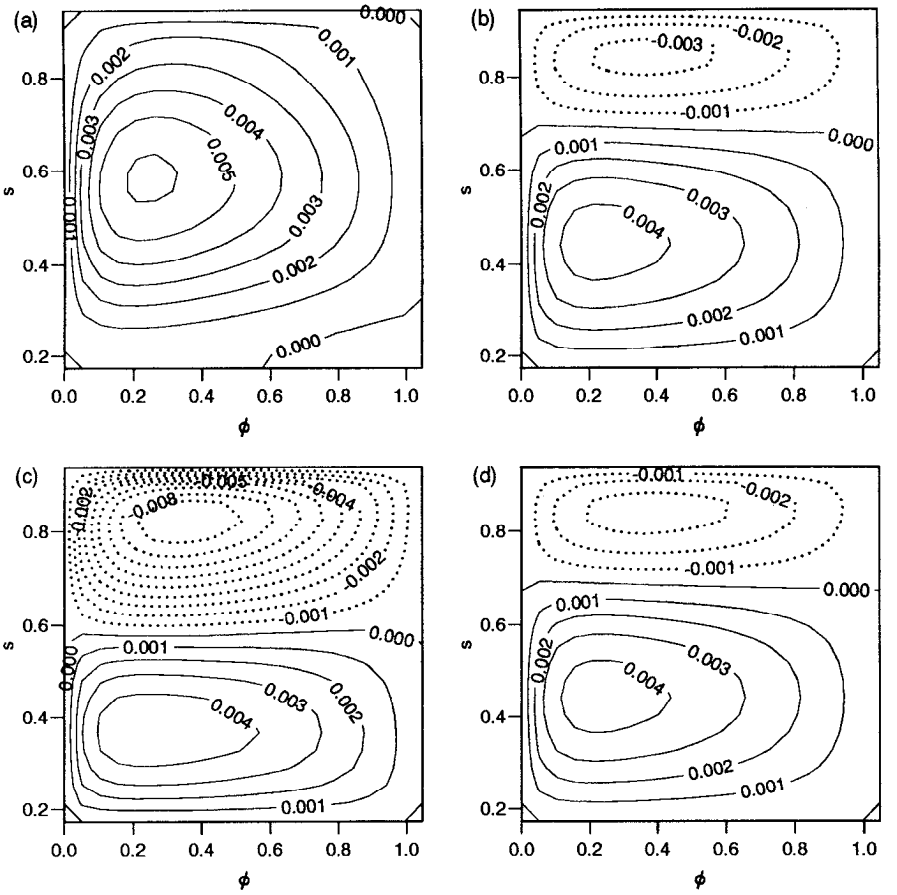

Figure 3. The barotropic stream function with period P equal to 1 year at; (a) $t = P/4$, (b) $t = P/2$, (c) $t = 3P/4$, (d) $t = P$. The scale is 1274 Sv.

derived from (58) is 0.18 Nm^{-2}. This is of the same order as the steady state wind stress, so the barotropic flow is radically altered during the cycle. Figure 3 shows the variation of the barotropic stream function. As expected from the discussion above, the effect of the thermal forcing at this oscillation frequency is small; removing it altogether led to alterations of less than one percent in the velocities and displacements, even at the point of minimum velocity perturbation. Immediately below the mixed layer at $t = 3P/4$, the extra vertical velocity induced by the additional oscillatory wind stress is very close to the expected peak dimensionless value of 0.025 throughout most of the domain. Mass conservation requires a compensatory upwelling but even lower down this return flow is confined to the southern and eastern regions of the model ocean, and to the other boundary points. We therefore define a subsection $\mathscr{D}$ of the model ocean by excluding the southern quarter of the s range and the eastern quarter of the ϕ range. Within the region $\mathscr{D}$ the analytical solution may have some applicability.

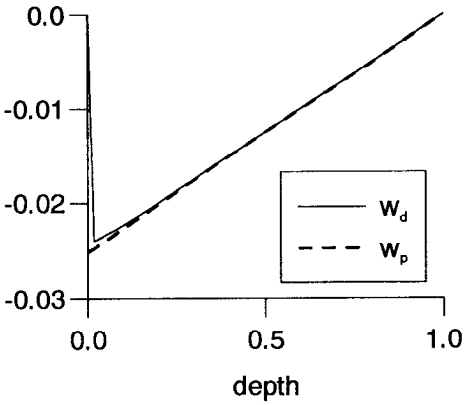

Figure 4. The vertical variation of the oscillatory part of the vertical velocity at $t = P/4$; w_d, along with the predicted value $w_p = 2\pi\epsilon_0 z/P$, at the center of the domain.

In the ideal fluid analytical solution, the temperature varies only by advection. The velocity responsible for the displacement is given by (19) with x and y replaced by the spherical coordinates ϕ and s. $\dot{\mathbf{x}}$ is linear in the sense that w is proportional to z, u is proportional to ϕ and v proportional to s. The resulting displacements of isosurfaces behave similarly.

To see whether the numerical solutions exhibit the same behavior, we first consider the times $t = P/4$ and $t = 3P/4$. At these times the isotherm displacement should pass through zero and changes in velocity compared to the steady state should be due only to the displacement velocity $\dot{\mathbf{x}}$, induced in the numerical model by the oscillatory wind stress. The velocity field from the numerical model is averaged over one cycle and subtracted from the velocity at $t = P/4$. The resulting velocity field $\mathbf{u}_d$ therefore corresponds to the maximum of displacement velocity $\dot{\mathbf{x}}$ which occurs at $t = P/4$. The extra vertical velocity w_d is very close to the predicted value throughout most of the domain, a compensatory return flow occupying the southern and eastern regions as noted above. The variation of w_d with z at the center of the domain is shown in Figure 4 along with the predicted value. The horizontal component of the additional velocity $\mathbf{u}_d$ can only be approximately fitted to the analytical solution over a limited region, as the presence of the boundaries in the numerical model causes the horizontal flow to recirculate in a basin scale gyre, as would be expected from the form of the stream function at $t = P/4$. However the horizontal part of $\mathbf{u}_d$ is very nearly constant in z below the mixed layer, as predicted.

In the numerical model changes in temperature will not be entirely due to advection, but examination of the magnitudes of terms in the dynamical equations for T and S shows that even in the steady state, advection is dominant throughout most of the solution. Diffusion in the vertical is a leading order term in the thermocline, but for rapid motions, changes of temperature are likely to be dominated by advection even there.

Confining attention to the region $\mathscr{D}$, the displacement velocity $\dot{\mathbf{x}}$ should have sinusoidal time-dependence $\sin(2\pi t/P)$ everywhere, while the resulting isosurface displacements

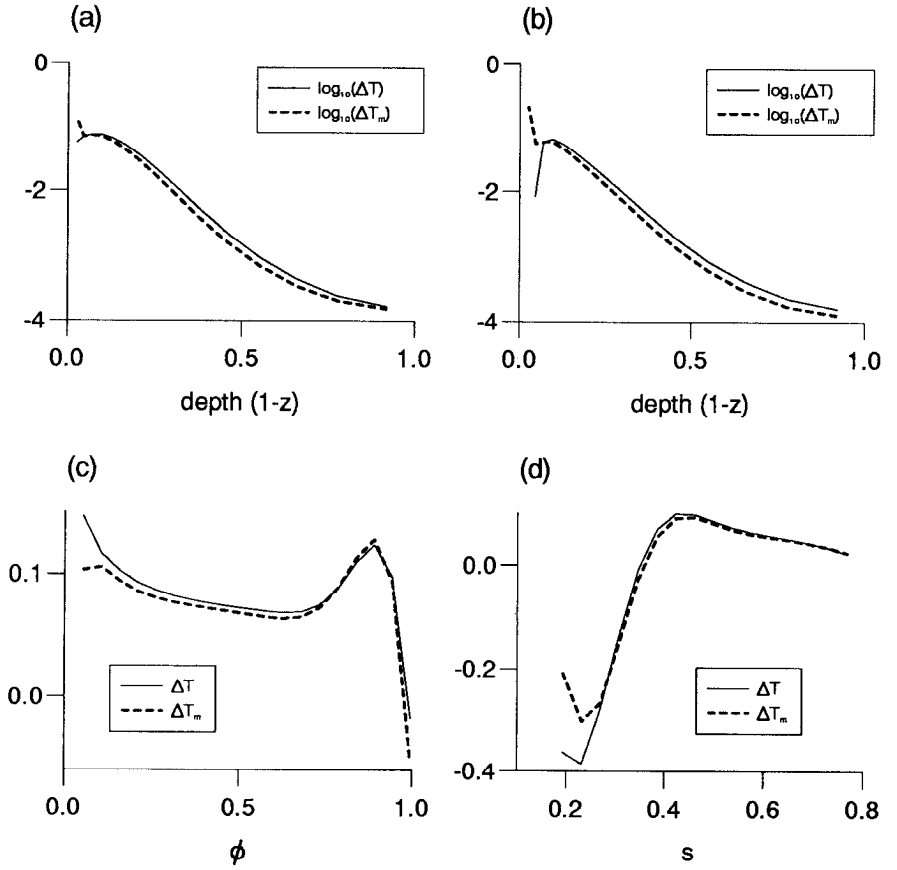

Figure 5. Variation of modeled (ΔT_m) and predicted (ΔT) maximum temperature changes along various sections for period $P = 1$ yr. A logarithmic scale is used to reveal the range of variation throughout the fluid column. The sections are (a) mid basin; (ϕ, s) = (0.52, 0.54), (b) Northwest; (ϕ, s) = (0.26, 0.73), (c) Upper thermocline; (s, z) = (0.54, 0.9), (d) Upper thermocline; (ϕ, z) = (0.52, 0.9).

should be proportional to cos ($2\pi t/P$). Analysis of the model solution suggests that the direction of the displacement velocity at a point does remain roughly constant throughout the cycle and that the phase of the oscillation is roughly as predicted. The amplitude of the (vector) displacement $\mathbf{d}$ at any point should therefore be equal to $P\mathbf{u}_d/2\pi$, assuming $\mathbf{u}_d$ corresponds to the amplitude of $\dot{\mathbf{x}}$ at each point. Since the displacements are small, the temporal variation of ∇T at a fixed point should also be small, in which case the amplitude of the periodic variation in temperature due to advection should be equal to

$$\Delta T = -\mathbf{d}.\nabla T. \tag{60}$$

In Figure 5 this estimate is compared with the difference ΔT_m between the model

temperature field at time $t = P/2$ (when the maximum displacement is predicted to occur) and the time-averaged field. Within $\mathscr{D}$ the temperature variations are typically slightly less than the predicted values, due presumably to the effects of diffusion, but otherwise the results suggest that the isotherms in the model solution are being displaced roughly in the manner predicted.

A feature of the numerical simulation which could not be predicted by the analytical solution is that the time-averaged state, about which the solution oscillates, is different from the steady state used to initialize the integration. This may be related to the phenomenon of nonlinear streaming mentioned in Section 4 whereby the periodic distortion leads to changes in the time-averaged mass and heat fluxes. In the bounded domain of the numerical model, additional interior fluxes must be balanced by changes in the boundary layers. This in turn will alter the interior flow, which is known to be fundamentally affected by the details of the boundary layers even in the linear regime (Pedlosky, 1969), although Salmon (1994) has suggested that this sensitivity is partly due to the unrealistically deep side wall layers in flat bottomed ocean models.

The time-averaged state, obtained by averaging over the last complete cycle, has less potential energy and more kinetic energy than the initial steady state. The dimensionless loss in potential energy (calculated as the integral of ρz over the entire domain) was 3.335×10^{-3}, while the kinetic energy increased from 3.233×10^{-2} to 4.899×10^{-2} (the energy scale is 7×10^{21} J). Within one cycle the potential energy changes by only about 6.043×10^{-5}, and the kinetic energy varies between about 4.75×10^{-2} and 5.61×10^{-2}, so the changes in the steady state are even larger than the amplitude of the oscillation. The continual oscillation of temperature surfaces probably acts to increase the vertical penetration of the surface heating, which occurs by vertical diffusion in the subtropical region. Cooling is carried out by vertical advection and convection in the north, and may be less strongly affected due to the weak stratification there. In this way the loss of potential energy might be linked to a deeper thermocline which is also manifested by an increase of 20 percent in the maximum of the zonally averaged overturning stream function. The actual picture is more complicated because in the upper half of the ocean, the averaged state does in fact have more potential energy than the initial steady state, possibly because stronger horizontal flows act to increase the effect of horizontal diffusion, which is a cooling influence there. At any rate the reduced density in the deep ocean outweighs this effect by a factor of two.

It is possible to consider the nonlinear streaming induced by the oscillations directly, by calculating the time-averaged velocity field and subtracting the velocity field associated with the time-averaged T and S fields. In the region $\mathscr{D}$ the differences are less than 0.1 percent of the velocities in the mean state, too small to be accurately resolved. In the return flow region to the east and south, an organized velocity streaming field occurs of a similar form to that induced in the upwelling phase of the oscillation, that is north eastwards at upper levels and south westwards at depth, with magnitude about one percent of the maximum value of $\mathbf{u}_d$ at a given level. The depth average of the streaming flow is

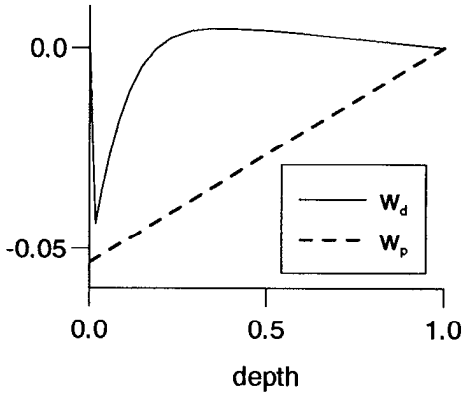

Figure 6. The vertical variation of the oscillatory part of the vertical velocity at t = P/4; w_d, along with the predicted value $w_p = 2\pi\epsilon_0 z/P$, at the center of the domain for the intermediate period case.

zero since the barotropic flow is constrained by the wind forcing. No such constraint applies to the meridional heat flux induced in the same way by the oscillation. Additional time-averaged heat fluxes, induced by the extra velocities, do occur as a result of the oscillation; the meridional component is northward in the upper levels and southward below. They add up to a net northward flux, averaged over time and over zonal sections, which decreases to the north and has a maximum amplitude of about 3.5 percent of the maximum zonally averaged meridional heat flux in the mean state.

b. Intermediate period. With the period of the forcing oscillation increased to about eight years, the character of the solution is quite different. Larger displacements are induced by a given displacing velocity $\dot{\mathbf{x}}$, so that even with the dimensionless displacement amplitude ϵ_0 increased from 0.001 to 0.017, (the depth of the top grid box, equivalent to about 70 m) the implied additional wind stress amplitude is still only 0.38 Nm^{-2}. As noted earlier this is deliberately large, but of a realistic order of magnitude. The maximum change in surface restoring temperature for this value of ϵ_0 is 3.5 K. Over a period of about 200 years the integration settles down to a uniformly periodic state, but in contrast to the results with annual forcing, parallels with the analytical solutions are strictly limited. This is clear from Figure 6 which is a comparison of diagnosed and predicted values of vertical velocity exactly analogous to Figure 4. The principal reason for this disagreement is the fact that the phase of the induced oscillation is a strong function of horizontal position. This is graphically illustrated by Figure 7 which shows the variation of temperature at z = 0.9 through one complete cycle as a function of zonal coordinate ϕ and time (ϕ covers the whole basin). Although the phase variations mean that the modeled ocean does not pass through its averaged state at all points simultanously, it is still interesting to calculate the velocity and meridional heat flux associated with this average state, and make comparisons with the time-averaged velocity and heat flux fields. Again the differences correspond to a form of nonlinear streaming induced by the oscillatory forcing. As for the annual period

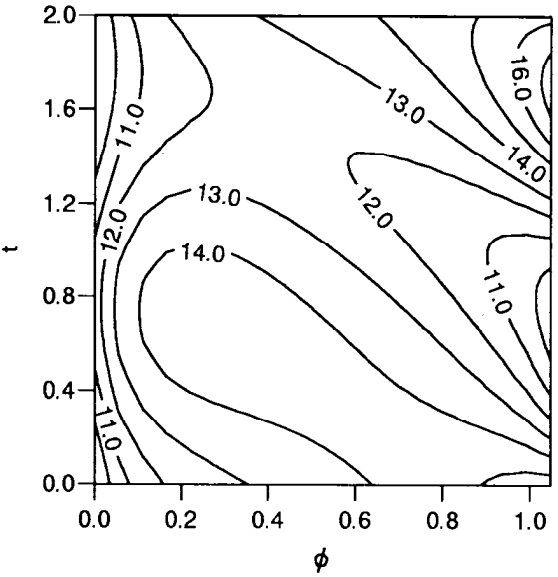

Figure 7. Model temperature as a function of time t and ϕ in the upper thermocline at (s, z) = (0.54, 0.9) for one complete cycle (the time scale is 4.04 years).

oscillations of smaller displacement amplitude, the streaming velocity is south-westward at depth and north-eastward at upper levels, but in this case it is less confined to the boundary regions and has measurable amplitude everywhere, peaking at two to five percent of the maximum velocity in the steady state at a given level. Again this flow can have no barotropic component, but can induce a nonzero time and zonally averaged meridional heat flux. In this case the induced meridional heat fluxes are a much larger fraction of the average values; the streaming velocity increases the maximum northward heat flux by over 10 percent and the peak value of the induced northward flux, which occurs at the southern boundary, is almost 50 percent of the peak northward flux in the averaged state. Since the time-averaged state is somewhat artificial, it may be more relevant to make comparisons with the initial steady state corresponding to the steady forcing. Compared to this state, the average northward heat flux is increased by 25 percent at its maximum value and 100 percent at the southern boundary.

c. Long period oscillations. For the final run to be discussed, the displacement amplitude ϵ_0 was again set to 0.017 while the period was increased to about 40 years. At this frequency and amplitude the changes in wind stress do not qualitatively alter the barotropic flow, but oscillations in wind and thermal forcings have a similarly strong impact on the solutions. This time the phase of the oscillation is roughly uniform on horizontal surfaces, but instead varies with depth. Time series of temperature in the center of the basin clearly show a temperature wave propagating downward through the thermocline, but the disturbance in the deep ocean is too weak to analyze.

Streaming velocities and additional meridional heat fluxes, calculated as before, are of a very similar form to the previous case but approximately ten times smaller. The same holds for the zonal average of the extra time-averaged heat fluxes. The heat fluxes implied by the steady state in this case are similar to those of the initial steady state. Note that the streaming velocities are still typically a factor of ten larger than the differences in velocity due to the residual unsteadiness of the oscillation.

9. Discussion of numerical results

The agreement between the numerical simulations and the analytical solution is greatest for annual period oscillations (much shorter periods are not appropriate to these dynamics). At longer periods the agreement deteriorates as the phase coherence of the oscillation is lost. This appears to be due to the westward propagation of long baroclinic Rossby waves. If the period is longer still, the propagation of disturbances from the eastern boundary may be rapid enough for the solution to reach approximate equilibrium, on the time scale of the oscillation. However, the propagation of information in the vertical still disrupts the phase of the oscillation. This is likely to be due to diffusion, neglected in the analytical solution, which would predict a decaying oscillation in the vertical with a vertical wavelength of about 0.25 of the ocean depth, for the parameters used. The observed vertical wavelength is closer to 0.4, but would be expected to be strongly modulated by advective effects.

It is possible to make an analytical estimate of the phase speed of long baroclinic Rossby waves to compare with the disturbances seen in Figure 7. At the latitude appropriate to the figure, the density gradient is fairly well fitted by the exponential function $\rho_z = Ae^{\gamma(z-1)}$, with $\gamma = 5.09$, $A = 13.8$, for which it can be shown that the fastest baroclinic wave mode has a dimensionless phase speed of about 0.71. Figure 7 appears to show disturbances propagating westward at a speed somewhat less than one and similar results are obtained with twice the period, reinforcing the conclusion that the disturbances correspond to Rossby waves.

Given that the annual oscillations are too fast for a baroclinic response mediated by long Rossby waves to occur, it is unsurprising that what is observed with annual forcing is essentially the instantaneous response to an applied wind stress. Horizontal velocity divergence in the directly wind-forced mixed layer produces roughly the intended Ekman pumping velocity. Incompressibility requires that this divergence is always in balance with upwelling from below, which can only arise as the divergence of a barotropic velocity field there. The roughly constant value of $\partial w/\partial z$ is an automatic consequence. Close to the eastern boundary this uniformity will break down due to baroclinic waves. The breakdown of the solution in the south may also be due to very strong downwelling at the southern boundary resulting from the unbalanced Ekman transport in the mixed layer. A better explanation is given by Gill and Niiler (1973) who predicted that the deep flow resulting from seasonal variations in surface forcing should be barotropic north of about 30N. In the more stratified waters nearer to the equator, they found that vertical motions could create significant baroclinic velocities above the main thermocline by changing the density

structure. They also predicted that annual changes in thermohaline fluxes at the surface would normally only affect local storage and that mean horizontal advection (which we ignored in calculating the oscillatory forcing) is not a dominant term. Note that the distortion velocity $\dot{x}$ in the analytical solution has a further special property, beyond merely being vertically uniform, which allows the solution to satisfy the thermal wind equations. Isotherms, or more generally isopycnals, are advected in such a way that the advecting velocity itself is the only source of time-dependence in the solution. That is, the solution is distorted along a locus of states, all of which would constitute steady solutions to the ideal thermocline equations in the absence of the distorting velocity. This is because the distorted steady state velocity field remains parallel to isopycnals. Unfortunately it is not straightforward to ascertain whether anything similar is occurring in the numerical solutions, partly because we have not attempted to model the changes in vertical velocity at the base of the mixed layer due to vertical advection of the steady solution. However, this is expected to be a small effect, so turning off the oscillatory forcing and finding the residual unsteadiness of the solution at various stages of the cycle does go some way toward investigating this point. We first restrict attention to a domain even smaller than $\mathscr{D}$ containing the most advective part of the solution and covering only half of the range of each of ϕ, s and z. Over this restricted region we calculate the r.m.s. of the instantaneous rates of change of all the dynamic variables in the model. For the initial steady state this measure of unsteadiness takes the value 2.6×10^{-3}, while for the annually oscillating solution the residual unsteadiness when the forcing is removed does not exceed 1.2×10^{-3} when either the distortion or the distorting velocity is maximal (that is for $t = 0, P/4, P/2, 3P/4$) but reaches 7.4×10^{-3} during the forced oscillation. Thus it appears, at least in a limited, highly advective region, that some of the essential character of the analytical solution is reproduced in this respect.

Some comments must be made on the effects of other differences between the model dynamics and those of the ideal fluid solution. We have so far made no specific comments about the effects of salinity. If we neglect diffusion and convection in the planetary geostrophic equations, then with any local form of constitutive relation $\rho(T, S)$, the temperature, salinity and density of fluid parcels will all obey the same pure advection equation in the interior of the fluid. Hence the inclusion of salinity can only affect how the modeled behavior of ρ, T or S resembles that of θ in the ideal fluid solution via the details of the diffusion; which must be small for any agreement to occur at all. The most important effect of salinity is therefore hopefully to render the initial steady solution, and the model dynamics in general, more realistic. Figure 8 shows the modeled and predicted variation of salinity with depth in exact analogy with Figure 5, confirming the prediction that salinity is behaving very similarly to temperature when the agreement with the ideal solution is good. Note that none of the oscillating numerical solutions induce extra convection, so its inclusion will not have affected the comparisons, other than by changing the initial steady state solution.

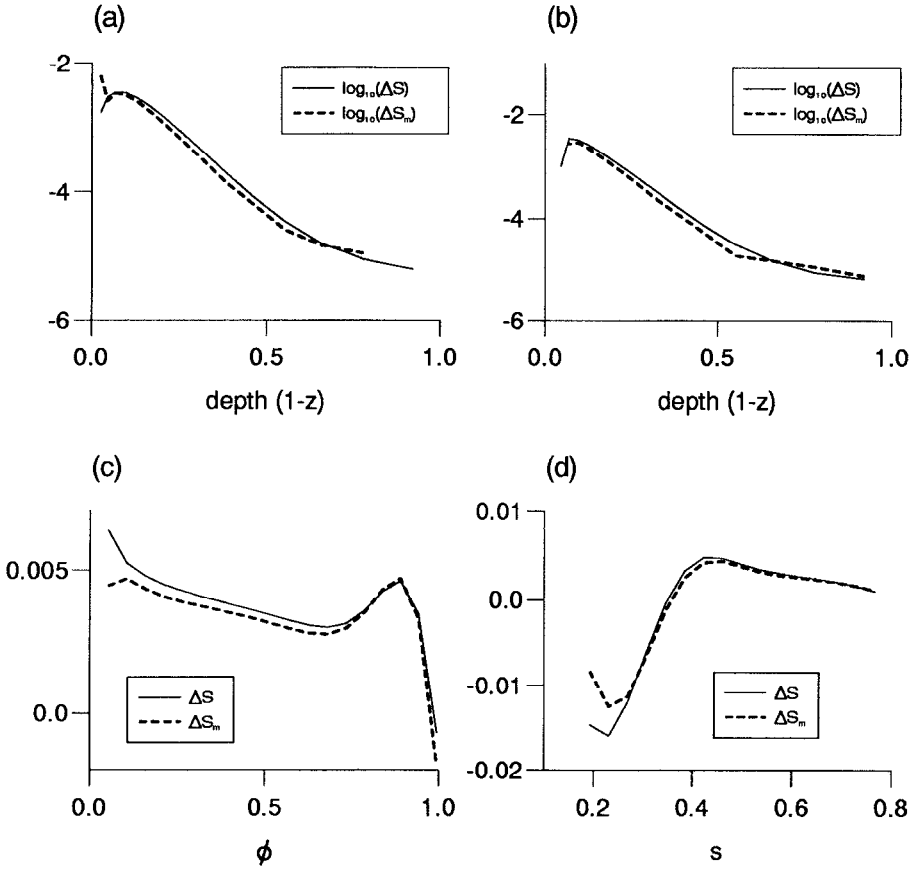

Figure 8. Variation of modeled (ΔS_m) and predicted (ΔS) maximum salinity changes along various sections for period $P = 1$ yr. A logarithmic scale is used to reveal the range of variation throughout the fluid column. The sections are (a) mid basin; (ϕ, s) = (0.52, 0.54), (b) Northwest; (ϕ, s) = (0.26, 0.73), (c) Upper thermocline; (s, z) = (0.54, 0.9), (d) Upper thermocline; (ϕ, z) = (0.52, 0.9).

10. Conclusions

An analytical solution of the unsteady ideal thermocline equations has been found which corresponds to distortion of the isopycnals of any given steady solution by an advecting velocity which varies linearly in the three coordinate directions. The temporal behavior is governed by a single arbitrary function of time. Potential vorticity, but not Bernoulli function, is also simply advected by the distorting velocity. Any advection equation has very general symmetries of this type, but for nonpassive quantities such as density, the distorting velocity is constrained to take a very special form. For the thermocline equations the constraints are satisfied by a distortion which has no thermal wind signature and in addition, can be seen to occur along a locus of steady states. The unsteady solution satisfies

similar boundary conditions to the steady solution which it generalizes and is unlikely to qualitatively alter its stability properties. For the example steady solution examined in Section 4, changes in internal energy caused by the time-dependence are associated with changes in thermocline depth and fluxes of energy from the western boundary.

The analytical solution has been compared with results obtained by applying a particular form of oscillatory forcing to a numerical model which integrates the planetary geostrophic equations in a box-shaped northern hemisphere basin. For annual period oscillations, certain features are reproduced by the model. The presence of western and northern boundaries prevents the horizontal flow from increasing linearly in the zonal and meridional directions, but otherwise the oscillatory part of the velocity field is similar to the analytical prediction. Changes in temperature and salinity are largely as predicted from the oscillating velocity field, particularly away from the eastern and southern boundaries. For longer periods the agreement breaks down due to the propagation of long waves from the eastern boundary. At still longer periods of around 40 years, it is the effect of vertical diffusion which disrupts the agreement. Thus the most likely physical application of the analytical solution is to annual fluctuations in thermocline depth. An important feature of the results which is predicted by the analytical solution, is that the oscillations induce changes in the time-averaged mass and heat fluxes of the steady state solution. These additional fluxes turn out to be negligible in some regions for annual forcing, but can be highly significant in general, for instance in altering the net meridional heat transport. This process is equivalent to the generation of turbulent fluxes by small scale eddies, but here the fluctuations are due to basin scale changes in forcing at periods of up to 40 years.

Acknowledgments. I wish to thank Peter D. Killworth and Andrew J. Willmott for helpful suggestions and discussion. Rick Salmon's input was also essential to the progress of the study, Simon Hood corrected some of my theoretical errors and Phillis Jones assisted with the figures. This work was supported by U. K. National Environment Research Council Grant GR3/8578.

APPENDIX A

The heat flux boundary condition

The no normal flow condition at lateral boundaries implies a linear relationship between the normal and tangential derivatives of density there. This makes it impractical to specify the derivatives of T or S at lateral boundaries. However, by postulating a distribution of diffusivity κ_H which tends to zero at the lateral boundaries, it may be possible to formulate a mathematical problem with no diffusive heat or salt flux across these boundaries, which has well behaved solutions. This requires some justification as the governing equations become singular where κ_H vanishes, however this does not preclude the existence of nonsingular solutions. As an example consider the model one-dimensional problem representing the solution close to a lateral boundary, resulting from neglecting time-dependence, convection and all variation tangential to the boundary. Referred to a

Cartesian coordinate x, normal to a boundary at $x = 0$, the heat Eq. (51) becomes

$$\kappa_H T_{xx} - uT_x + \gamma T = 0, \tag{A1}$$

where the subscript denotes a derivative and the γ term parameterizes all the neglected variations. Now suppose the x-variations of κ_H, u and γ are such that (A1) can be written as

$$x^2 T_{xx} + xq(x)T_x + r(x) = 0. \tag{A2}$$

Solutions to (A2) can be found close to its singular point at zero using the method of Frobenius, see for example Kreider *et al.* (1966), if q and r are analytic near zero ($r(0)$ can be zero). For certain choices of q and r, one or both of the two linearly independent solutions to (A2) will be nonsingular at zero. In particular (expanding q and r as e.g. $q = q_0 + q_1 x + q_2 x^2 + \cdots$) if we set $q(x) = q_0 + q_1 x$ with $0 < q_0 < 1$ and $r(x) = r_1 x$, then the equation has two linearly independent, nonsingular solutions of the form

$$T = \sum_{k=0}^{\infty} a_k x^{k+\nu}. \tag{A3}$$

$\nu = \nu_1, \nu_2$ are the two solutions of

$$I(\nu) = \nu(\nu - 1) + q_0 \nu + r_0 = 0, \tag{A4}$$

which in this case are 0 and $1 - q_0$, and the a_k are given by

$$a_k = -\frac{1}{I(k + \nu)} \sum_{j=0}^{k-1} [(j + \nu)q_{k-j} + r_{k-j}]a_j, \qquad k > 0, \tag{A5}$$

for $\nu = \nu_1, \nu_2$. Either of these solutions can be matched to an interior solution at a point $x = x_1$ where T, κ_H, u and γ take prescribed interior values T_1, κ_1, u_1 and γ_1 by setting $r_1 = \gamma_1 x_1^2/\kappa_1$ and $q_1 = -u_1/\kappa_1 - q_0/x_1$. The solution with $\nu = 0$ has a nonzero value of T at the boundary and both solutions satisfy $\kappa T_x = 0$ there.

The existence of such nonsingular solutions to the model one-dimensional problem suggests that there are nonsingular solutions to a three-dimensional problem in which κ_H is constant in the interior and approaches zero in some way close to boundaries, possibly in proportion to the squared distance from the boundary as above. This would explain how numerical solutions are readily obtained, and indicate how they might be made resolution independent, by incorporating the variation in κ explicitly.

REFERENCES

Bluman, G. W. and S. Kumei. 1989. Symmetries and Differential Equations. Springer-Verlag, Berlin 412 pp.

Cai, W. J. 1995. Interdecadal variability driven by a mismatch between surface flux forcing and oceanic freshwater/heat transport. J. Phys. Oceanogr., *25,* 2643–2666.

Charney, J. G. and M. Stern. 1962. On the stability of internal baroclinic jets in a rotating atmosphere. J. Atmos. Sci., *19,* 159–172.

Clarkson, P. A. and M. D. Kruskal. 1989. New similarity solutions of the Boussinesq equations. J. Math. Phys., *30,* 2201–2213.

Colin de Verdière, A. 1988. Buoyancy driven planetary flows. J. Mar. Res., *46,* 215–265.

—— 1989. On the interaction of wind and buoyancy driven gyres. J. Mar. Res., *47,* 595–633.

de Szoeke, R. A. 1995. A model of wind-driven and buoyancy-driven ocean circulation. J. Phys. Oceanogr., *25,* 918–941.

Filippov, U. G. 1968. Application of invariant-group method to solution of the problem of non-homogeneous ocean current determination. Meteorologiia i Gidrologiia, *9,* 53–62 (in Russian).

Gill, A. E. 1982. Atmosphere-Ocean Dynamics., Intl. Geophys. Ser., *30,* Academic Press, NY, 662 pp.

Gill, A. E. and P. P. Niiler. 1973. The theory of seasonal variability in the ocean. Deep-Sea Res., *20,* 141–177.

Head, A. K. 1993. Lie, a pc program for Lie analysis of differential equations. Comp. Phys. Comm., *71,* 241–248.

Killworth, P. D. 1983. Some thoughts on the thermocline equations. Ocean Model., *48,* 1–5, (unpublished manuscript).

—— 1987. A continuously stratified nonlinear ventilated thermocline. J. Phys. Oceanogr., *17,* 1925–1943.

Kreider, D. L., D. R. Ostberg, R. G. Kuller and F. W. Perkins. 1966. An introduction to linear analysis, Addison-Wesley, Reading, MA. 773 pp.

Luyten, J., J. Pedlosky and H. Stommel. 1983. The ventilated thermocline. J. Phys. Oceanogr., *13,* 292–309.

Niiler, P. P. and P. S. Dubbelday. 1970. Circulation in a wind-swept and cooled ocean. J. Mar. Res., *28,* 135–149.

Olver, P. J. 1986. Applications of Lie Groups to Differential Equations, Springer-Verlag, Berlin 497 pp.

Pedlosky, J. 1969. Linear theory of the circulation of a stratified ocean. J. Fluid Mech., *35,* 185–205.

—— 1987. Geophysical fluid Dynamics, Springer-Verlag, Berlin 710 pp.

Rahmstorf, S. 1993. A fast and complete convection scheme for ocean models. Ocean Model., *101,* 9–11, (unpublished manuscript).

Rahmstorf, S. and J. Willebrand. 1995. The role of temperature feedback in stabilizing the thermohaline circulation. J. Phys. Oceanogr., *25,* 787–805.

Salmon, R. 1990. The thermocline as an "internal boundary layer." J. Mar. Res., *48,* 437–469.

—— 1994. Generalized 2-layer models of ocean circulation. J. Mar. Res., *52,* 865–908.

Salmon, R. and R. Hollerbach. 1991. Similarity solutions of the thermocline equations. J. Mar. Res., *49,* 249–280.

Welander, P. 1971. Some exact solutions to the equations describing an ideal-fluid thermocline. J. Mar. Res., *29,* 60–68.

Winton, M. and E. Sarachik. 1993. Thermohaline oscillations induced by strong steady salinity forcing of ocean general circulation models. J. Phys. Oceanogr., *23,* 1389–1410.

Young, W. R. and G. R. Ierley. 1986. Eastern boundary conditions and weak solutions of the ideal thermocline equations. J. Phys. Oceanogr., *16,* 1884–1900.

Zhang, S., R. J. Greatbach and C. A. Lin. 1993. A reexamination of the polar halocline catastrophe and implications for coupled ocean-atmosphere modeling. J. Phys. Oceanogr., *23,* 287–299.

Received: *8 August, 1995;* revised: *11 June, 1996.*